J Nanostruct 16(3): 3761-3770, Summer 2026

RESEARCH PAPER

Experimental Study the Corrosion Resistance and Wear Resistant of (Ti12Mo) alloy by Alumina particles addition Using Powder Metallurgy for Humans Implant

*Saleh Jawad Hamza *, Ahmed Mousa Marheb, Hasan A. Abbas Alhilali*

Department of Materials Engineering, College of Engineering, University of Al-Qadisiyah, Iraq

ARTICLE INFO

Article History:
Received 14 March 2026
Accepted 07 June 2026
Published 01 July 2026

Keywords:
Biomaterials
Corrosion resistance
Nano
Orthopedics
Rate of wear

ABSTRACT

This study experimentally investigates the influence of alumina (Al_2O_3) particle reinforcement on the corrosion resistance and wear performance of a Ti–12Mo alloy fabricated via powder metallurgy for potential orthopedic implant applications. Elemental titanium and molybdenum powders were blended to obtain a Ti–12Mo composition and reinforced with Al_2O_3 at amounts ranging from 0.5 to 5 wt.%. The powder mixtures were mechanically mixed for 5 h, compacted at 800 MPa into disc-shaped specimens, and sintered at 950 °C for 7 h under an argon atmosphere. Phase constitution and microstructural evolution were characterized using X-ray diffraction and scanning electron microscopy. Electrochemical corrosion behavior was evaluated in Ringer's solution at 37 ± 1 °C using potentiodynamic polarization, while dry sliding wear behavior was assessed using a pin-on-disk apparatus under applied loads of 10 and 20 N. The results demonstrate that increasing Al_2O_3 amount significantly enhances densification, leading to a reduction in porosity from 34.4% for the base alloy to 19.2% at 5 wt.% Al_2O_3. Consequently, the corrosion resistance of Ti–12Mo was markedly improved, with the corrosion rate decreasing to 2.14×10^{-10} mpy and an enhancement efficiency of 98.8% at 5 wt.% Al_2O_3. In parallel, Al_2O_3 reinforcement substantially enhanced resistant to wear, achieving a maximum enhancement of 98. % at 5 wt.% Al_2O_3, corresponding to a rate of wear of 1.26×10^{-8} $cm^3/N{\cdot}m$. The enhancement in tribological performance is attributed to increased hardness (up to ~295 kg/mm^2), reduced porosity, and the formation of strengthening intermetallic phases within the Ti–Mo matrix.

How to cite this article
Jawad Hamza S, Mousa Marheb A, A. Abbas Alhilali H. Experimental Study the Corrosion Resistance and Wear Resistant of (Ti12Mo) alloy by Alumina particles addition Using Powder Metallurgy for Humans Implant. J Nanostruct, 2026; 16(3):3761-3770. DOI: 10.22052/JNS.2026.03.063

INTRODUCTION

Titanium and its alloys remain the traditional backbone of load-bearing biomedical implants because they combine low density, high specific strength, and excellent corrosion resistance that originates from the rapid formation of a stable passive TiO_2 film in physiological environments [1–5]. Nevertheless, widely used alloys (e.g., conventional α/α+β systems) may present a mechanical mismatch with bone due to their relatively high elastic modulus, which can promote stress shielding and long-term loosening

* *Corresponding Author Email: salehjawadhamza@qu.edu.iq*

[6,7]; therefore, modern implant metallurgy has increasingly focused on β-type titanium alloys engineered to achieve lower modulus while retaining high corrosion stability and adequate strength [8]. Among β-stabilizing elements, molybdenum is widely adopted because it strongly stabilizes the β phase and is commonly associated with improved passivation and corrosion performance in chloride-containing media [9–11], which makes Ti–Mo compositions (including Ti–12Mo-class alloys) attractive candidates for next-generation orthopedic components [12]. However, a persistent limitation of titanium alloys in demanding implant locations is their modest tribological behavior—typically low hardness and poor resistant to wear—which can accelerate material loss and increase the risk of debris-related biological complications [13]; hence, improving wear/tribocorrosion performance remains a central requirement for extending implant service life [14].

A proven pathway to address titanium's tribological weakness is to develop titanium matrix composites by incorporating hard ceramic particulates that increase load-bearing capability at the contact interface and reduce the real area of metallic adhesion [14–16]. Alumina (Al_2O_3) is especially attractive because it is chemically inert, hard, and commonly considered compatible for biomedical use, while its incorporation can markedly enhance resistant to wear and may also modify corrosion and tribocorrosion response through microstructural and interfacial effects. Recent tribocorrosion studies on Ti–Al_2O_3 composites processed via powder routes have demonstrated that alumina additions can influence both electrochemical behavior and material degradation under combined mechanical–electrochemical loading in saline solutions relevant to physiological conditions [17].

Powder metallurgy (PM) is particularly suitable for producing Ti–Mo-based composites because it offers near-net-shape manufacturing, compositional flexibility, and the ability to distribute reinforcement particles more uniformly than many melt routes, while also enabling microstructure and porosity tailoring when required for biomedical function [18,19]. Over the last decade, PM of titanium alloys has been repeatedly highlighted as a cost-effective and technically mature pathway for structural and biomedical titanium components, with strong emphasis on its advantages in near-net-shape fabrication and property tailoring [20]. Despite these advances, the coupled corrosion–wear response of PM-processed Ti–Mo alloys reinforced with Al_2O_3 remains insufficiently established in the open literature compared with the extensive work on monolithic alloys or surface-engineered titanium. In particular, systematic experimental evidence clarifying how alumina particulates affect microstructure, densification quality, passive-film stability, and wear/tribocorrosion mechanisms in Ti–Mo matrices is still needed to guide implant-oriented material selection and processing optimization [14].

Recent studies have clearly advanced the understanding of titanium-based biomaterials; however, important limitations remain. Zhang and Chen [21] comprehensively reviewed biomedical titanium alloys and confirmed that β-type Ti alloys, including Ti–Mo systems, exhibit superior corrosion resistance and lower elastic modulus than conventional Ti alloys, yet they emphasized that poor resistant to wear remains unresolved for load-bearing implant applications.

Table 1. The physical properties of the powdered materials utilized in this experiment.

Powders	Ti	Mo	Al_2O_3
Average particle size(μm)	26.43	29.89	5.325
Purity %	99.85	99.90	99.98

Table 2. Composition of the etching solution [25].

NO	Constituents	Ml
1	HF	10 ml
2	HNO_3	5 ml
3	H_2O	85 ml

Zhou et al. [22] experimentally demonstrated that powder-metallurgy-processed Ti–Mo alloys show improved passivation behavior and reduced corrosion current density in phosphate-buffered saline as Mo amount increases; nevertheless, their work focused on monolithic alloys without addressing tribological degradation. Fang et al. [20] and Wang et al. [23] highlighted that powder metallurgy enables near-net-shape fabrication and compositional flexibility for biomedical titanium, but both studies reported that residual porosity and limited surface hardness still constrain wear performance. To overcome this, Sousa et al. [17] investigated Ti–Al_2O_3 composites produced via powder routes and showed that alumina reinforcement significantly enhances resistant to wear and modifies tribocorrosion behavior in saline media; however, their matrix systems were primarily pure Ti or Ti–Al based, not β-Ti alloys. More recently, Sousa et al. [24] further demonstrated that Al_2O_3 amount and interfacial phases strongly influence corrosion and tribocorrosion mechanisms, yet Ti–Mo matrices were not considered. Collectively, these studies reveal a clear gap: although Ti–Mo alloys are well recognized for corrosion stability and Al_2O_3 reinforcements are proven to improve resistant to wear, there is a lack of systematic experimental research integrating both strategies—specifically, the corrosion and wear behavior of powder-metallurgy-fabricated Ti–12Mo alloys reinforced with alumina particles—along with a mechanistic correlation between densification, microstructure, passive-film stability, and wear mechanisms under conditions relevant to human implants.

MATERIALS AND METHODS

The samples have been produced by powder metallurgy using Ti12Mo-xAl_2O_3 alloys. Table 1 provides the specimen's mean particle size and purity level. Steel balls of various sizes were used in a revolving motorized ball mill to carefully combine the weighted powders. As a wet blending medium, ethanol has been utilized. Five hours were spent on the blending process. An electrical hydraulic press was used to compress a 3.5-gram powder mixture of fine particles to produce a disk-shaped specimen that measured diameter=1.2 cm and thickness= 0.6 cm. Throughout compaction, 800 MPa of pressure had been used, and the specimen was kept at this pressure for four minutes. Under argon situations, the process of sintering has been carried out in an electrical argon oven. Following the compaction phase, the specimens were sintered by raising their temperature to 950 ˚C at a rate of 10 ˚C per minute. After being submerged for seven hours, the samples are cooled in the oven until they reach room temperature.

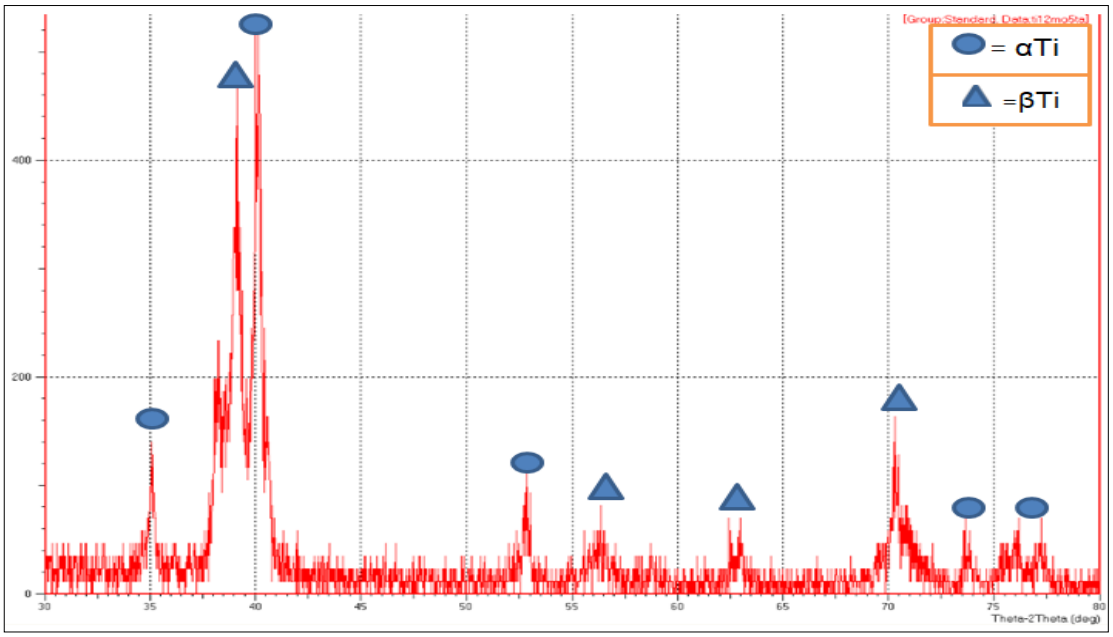

Fig. 1. shows the XRD patterns of Ti12Mo after the process of sintering.

Microstructures Characterization

X-Ray Diffraction

Following sintering, the Ti alloy was examined using X-ray diffraction, and the results had been in comparison with typical charts. With a copper (Cu) target, the test has been carried out at a speed of 6°/min, a step size of 0.02°, and with an angle ranging from 20 to 80 °. The voltage was 40 kilovolts, the current had been 30 mA, and the wavelength used had been 1.54060 Angstroms.

Microstructure Observation

Following sintering, silicon carbide sheets with different grit sizes—180, 400, 600, 800, 1000, 1200, 1500, and 2000—were used to grind all of the specimens. The last step was polishing the specimens utilizing diamond paste to get a glossy

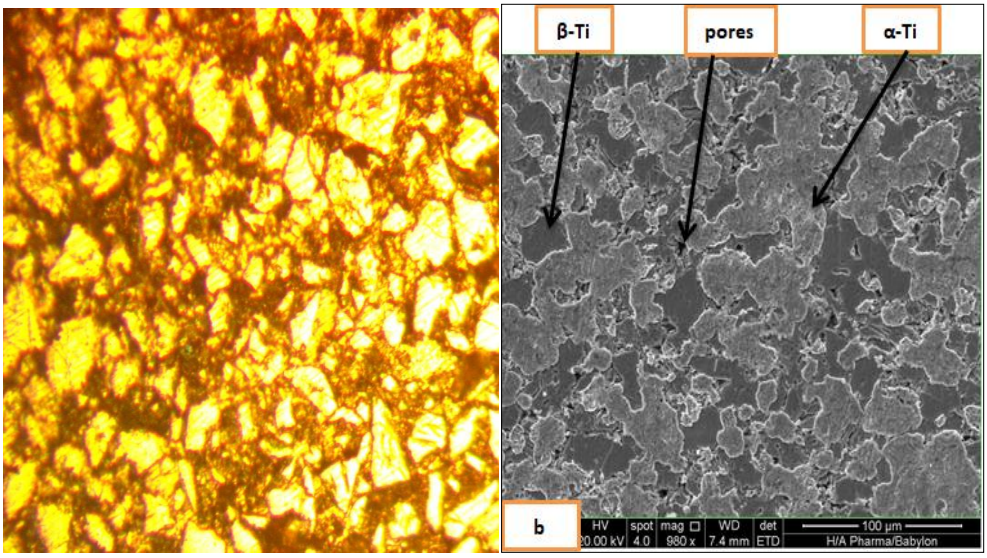

Fig. 2. The base's microstructure observation. a) Making use of the 400X optical microscope. c) Using the SEM.

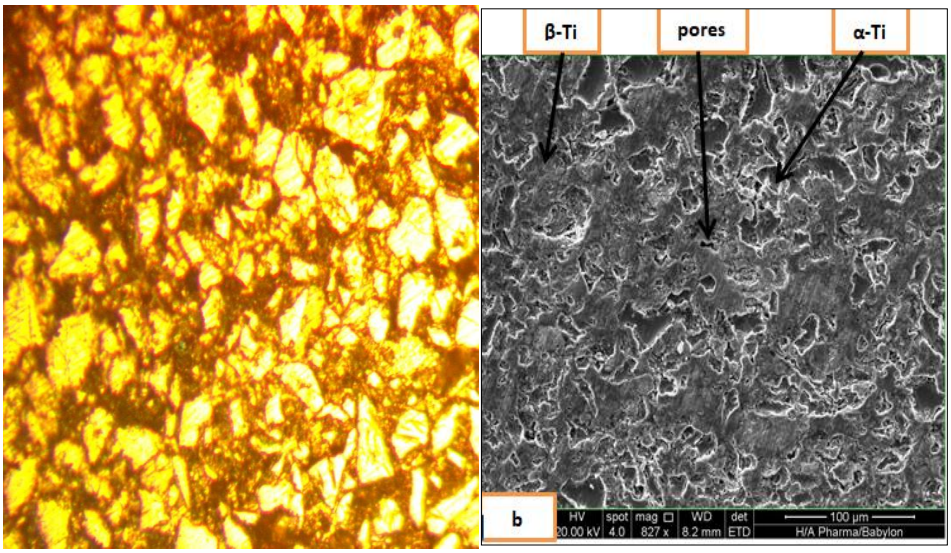

Fig. 3. The microstructure observation of the 2.5% Al_2O_3 addition; a) Making use of the 400X optical microscope. b) Using the SEM.

and shiny appearance. The room temperature was used for the etching process. The chemical makeup of the etching solution is shown in Table 2 [25]. The specimens were cleaned with water and dried after the etching procedure. After that, optical and scanning electron microscopy were used to examine them at 400x magnification. The examination of grain boundaries includes characteristics including grain size, shape, and phase identification. Each of them has characteristics.

Corrosion Test

In compliance with ASTM guidelines, polarization studies were carried out using an electrochemical standard cell that included a reference electrode (saturated calomel electrode) in Ringer solution, an auxiliary electrode (platinum), and a working electrode [26]. A potentiostat of the Winking M Labf200 type has been used for polarization experiments. Potentiodynamic polarization begins at an initial potential of 250 mV under the open circuit potential and proceeds to 800 mV above the open circuit potential after achieving a constant potential. The current was measured in proportion to the potential after the samples had been scanned in the positive direction at a sweep rate of 0.4 mV/s. The Eq. 1 is used to compute the corrosion rate after the test yields the corrosion current density (Icorr) and corrosion potentials (Ecorr) [26].

$$\text{Corrosion Rate (mpy)} = \frac{0.13 i_{corr} (\text{E. W.})}{\rho} \quad \textbf{(1)}$$

Whereas, E.W: equivalent weight (g/eq.), ρ: density (g/cm^3), Icorr: current density (μA/cm^3).

Wear Test

Pin-on-disk devices (MT-4003, version 10) are used to study dry sliding wear. 300 rpm, a constant radius of 4 mm, varying sliding distances, and loads of 10N and 20N were used in the test. An electrical scale with a 0.0001 precision is used to weigh the sample before testing. The samples are scaled at set times (5, 10, 15, 20, 25, and 30 min), and the dry sliding rate of wear is computed using Eq. 2. The test procedure was conducted in accordance with ASTM G 99 [27,28].

$$V_{loss} = \frac{\Delta W}{\rho} \quad (2)$$

Whereas, ΔW= The weight loss (g) after 5, 10, 15, 20, 25, and 30 minutes, ρ (g/cm^3) = final

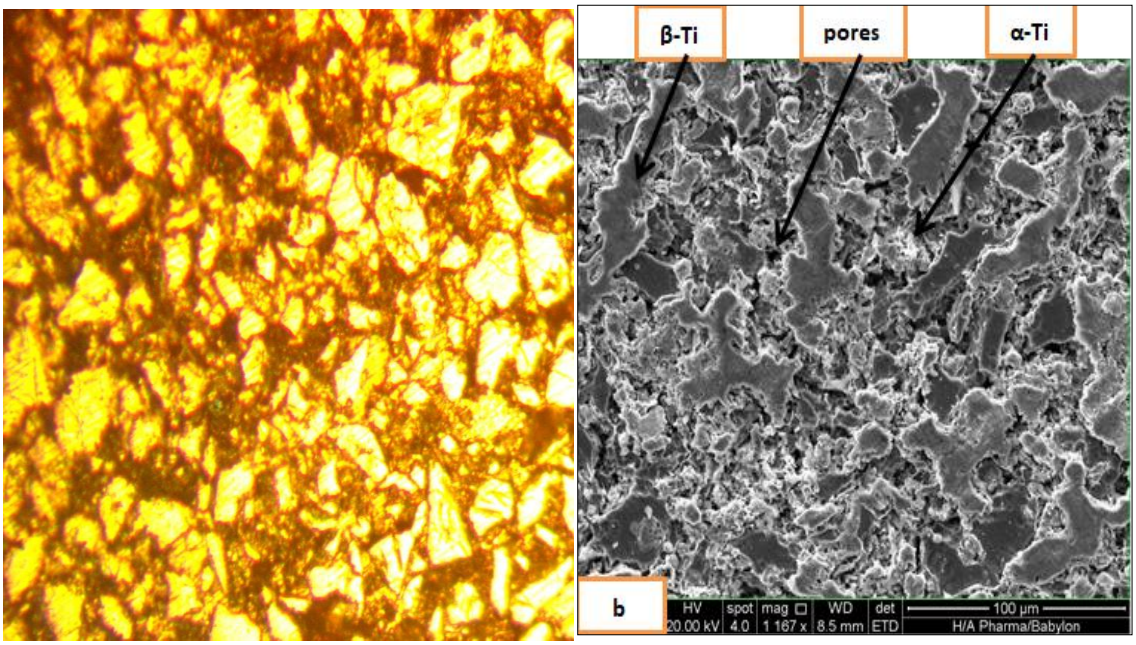

Fig. 4. The microstructure observations of the 5% Al_2O_3 addition: a) Making use of the 400X optical microscope; b) Using the SEM.

density.

The rate of wear has been determined from Eq. 3 [29].

$$W_a = \frac{\Delta G}{\rho P s} \quad (3)$$

Whereas, W_a refers to the rate of wear, (cm^3/N.m), ΔG refers to the loss in weight, (g), ρ refers to the density of the selected materials, (g/cm^3), P refers to the applied load, (N), s refers to the distance of sliding, (m).

RESULTS AND DISCUSSION

Microstructure Characterization

The observable elements in the XRD patterns of the green compact alloys are the Al_2O_3 phases of alumina particles, titanium (Ti), molybdenum (Mo). This is due to the fact that phase transition does not occur during the compacting process. One kind of process of diffusion that needs an elevated temperature to occur is phase transition. The XRD patterns formed by the base alloy (Ti12Mo) during sintering at 950 degrees Celsius for seven hours in an argon environment are shown in Fig. 1. Two

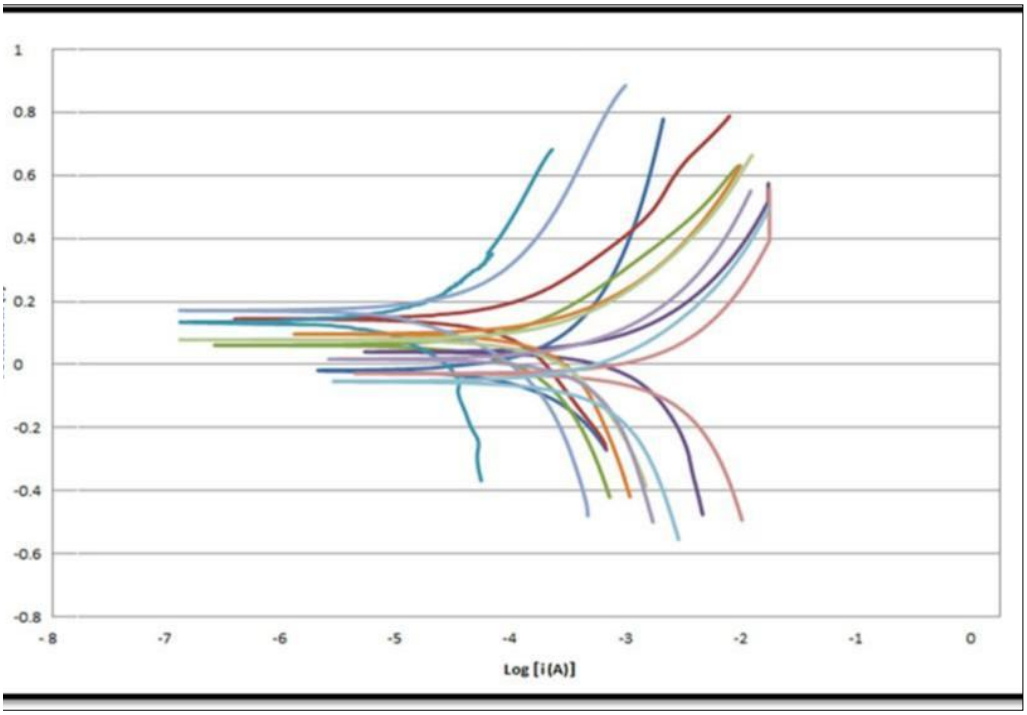

Fig. 5. The Leaner polarizing curves for the base alloy and the base alloy with Al_2O_3 addition.

Table 3. the porosity, corrosion current density (Icorr), corrosion potential (Ecorr), enhancement rate, and the rate of corrosion.

Al_2O_3 (%)	Porosity (%)	$I_{corr.}$ (μA/cm^2)	$E_{corr.}$(mv)	Rate of corrosion (C.R) mpy	Enhancement rate (%)
0	34.4	1.58 x10^{10}	-298	1.90x10^{8}	-
0.5% Al_2O_3	33.7	3.10 x10^{10}	-220	1.89x10^{8}	0.45%
1% Al_2O_3	31.4	1.80 x10^{11}	-180	6.10 x10^{9}	70%
1.5% Al_2O_3	29.2	8.33 x10^{11}	-175	4.20x10^{9}	75%
2% Al_2O_3	27.4	7.55 x10^{11}	-160	3.76 x10^{9}	78%
2.5% Al_2O_3	26.6	4.10 x10^{11}	-155	3.50 x10^{9}	79%
3% Al_2O_3	24.9	2.00 x10^{11}	-149	3.10 x10^{9}	813%
3.5% Al_2O_3	23.2	4.17 x10^{11}	-120	2.43 x10^{9}	85%
4% Al_2O_3	22.6	2.23 x10^{11}	-89	1.66x10^{9}	90%
4.5% Al_2O_3	21.1	5.25 x10^{12}	-31	4. 0 x10^{10}	97%
5% Al_2O_3	19.2	2.23 x10^{12}	-11	2.14 x10^{10}	98%

solid solutions, αTi and βTi, were formed from Mo, and Ti.

The base alloy (Ti12Mo) with 5 percent Al_2O_3 XRD pattern is shown in Fig. 1 after a 7-hour sintering operation at 950 degrees Celsius in an argon gas environment. The fundamental elemental chemicals Ti, Mo, and Al_2O_3 are transformed into αTi, βTi, and Ti6 Al_2O_3 in the image. Nevertheless, there are no peaks in the image that correspond to metal Ti, Mo, and Al_2O_3. Because it improved the interdiffusion between Al_2O_3, Mo, and Ti, the 7-hour sintering procedure was enough to finish the phase transformation process. Because unbound elements have negative impacts on the body, they are prevented in alloys utilized as biomaterials.

At a 400X magnification, the etched alloys microstructure after the process of sintering is shown in Figs. 2-4, both with and without the inclusion of Al_2O_3. By looking at these alloys' microstructure, the boundaries of the grains and the current phases were determined. Following the process of sintering, the samples were discovered to have a duplex microstructure, which is made up of two separate areas. The α-Ti phase is present in one area, which looks light (bright), whereas the β-phase is present in the other parts, which seem dark. Because Mo elements stabilize the β phase, their existence causes the dark reign (β-phase) to be promoted. The darkened area rises as the number of alumina particles increases. Similar to α-β and β alloys, certain beta phases are in equilibrium at room temperature [30]. Granular boundaries, pores of different sizes, and the α-Ti and β-Ti phases are visible in the SEM images of the etched alloys, which can be seen in Figs. 2-4. A limited number of surface holes are seen by the SEM inspection because of the metal powder approach employed to prepare the sample; these pores diminish as the quantity of alumina particles rises. The material's resistance to corrosion is improved by this decrease in porosity, which is ascribed to the function of alumina particles in altering the alloy structure. The homogeneous distribution of the reinforcing phase during the matrix produced by the powder metallurgy method improves the mechanical properties and resistant to wear of the alloys used. As shown in XRD Fig. 1, the microstructure exhibits the presence of an intermetallic phase (α-Ti - β-Ti), which improves the alloy's mechanical characteristics and hardness as the amount of alumina particles increases.

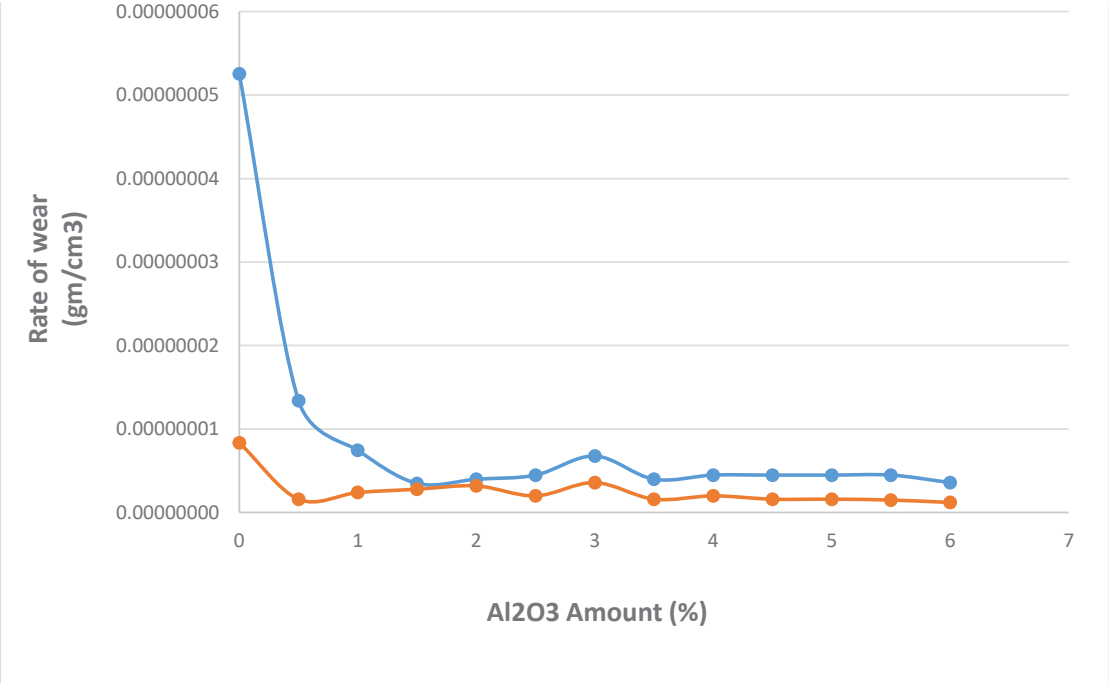

Fig. 6. The effect of Alumina particles (10N,20N) amount on rate of wear.

Corrosion Test

A single specimen of every (Ti12Mo-x Al_2O_3 and Ti12Mo) was used in the electrochemical corrosion process. Fig. 5 shows the anodic and cathodic polarization properties of Ti12Mo-x Al_2O_3 and Ti12Mo in Ringer solution at 37±1 degrees Celsius using schematic current-potential curves, sometimes referred to as polarization curves. The polarizing curves for the Ti12Mo alloy and the Ti12Mo alloy with Al_2O_3 addition are shown in Fig. 6. When cathodic polarization occurs, the voltage increases and the current decreases until it reaches the lowest possible magnitude. The voltage increases as the current increases throughout anodic polarization. The concurrent rise in voltage and current is indicative of active anodic polarization activity, which shows that the metal is still dissolving. The anodic curve's form shows that both the Ti12Mo alloy and the Ti12Mo alloy with Al_2O_3 addition have a passive area. Fig. 6 shows the corrosion current densities, corrosion potentials, and the calculated rate of corrosion information derived from these curves.

Table 3 clearly demonstrates a pronounced and systematic enhancement in the corrosion resistance of the base Ti–12Mo alloy with increasing Al_2O_3 amount, which is closely associated with the progressive reduction in residual porosity. The corrosion resistance enhancement increases from a marginal 0.5% at 0.45 wt.% Al_2O_3 to 70. % at 1 wt.%, 75% at 1.5 wt.%, and exceeds 78% beyond 2 wt.% Al_2O_3, ultimately reaching a maximum enhancement of 98% at 5 wt.% Al_2O_3. This trend is corroborated by the electrochemical parameters, as the corrosion current density (I_{corr}) decreases markedly from 3.10×10^{-10} μA/cm^2 at 0.5 wt.% Al_2O_3 to 2.23×10^{-12} μA/cm^2 at 5 wt.% Al_2O_3, both of which are substantially lower than that of the unreinforced alloy (1.90×10^{-10} μA/cm^2). Concurrently, the corrosion potential (E_{corr}) shifts progressively toward more noble values, from −220 mV at 0.5 wt.% Al_2O_3 to −11 mV at 5 wt.% Al_2O_3, compared with −298 mV for the base alloy. The combined decrease in I_{corr} and positive shift in E_{corr} indicate enhanced passivation behavior, which can be attributed to porosity reduction and the formation of a more compact and stable protective oxide layer on the alloy surface induced by Al_2O_3 addition, thereby effectively suppressing electrochemical dissolution and improving corrosion resistance.

Wear Test

The association between enhanced resistant to wear and a higher Al_2O_3% indicates that the addition of Al_2O_3 improves resistant to wear. The creation of the intermetallic complex (Ti6 Al_2O_3), which adds to the enhanced hardness of all alloys having germanium, is responsible for this occurrence. The Brinell hardness (HB) and resistant to wear enhancement % of the Ti12Moalloy in relation to the addition of Al_2O_3 are shown in Table 4. The rate of wear for Ti12Mo alloy is ($2.20\text{x}10^{-6}$, $4.10\text{x }10^{-6}$) (cm^3/N.M) at (10N & 20N), respectively. The above statistics show that when loads of 10N and 20N are applied, the rate of wear at (20N) is higher than that of (10N) due to an increased friction coefficient. Before reaching its maximum value, the rate of wear first rises between 10N and 20N. Nevertheless, the rate of wear stabilizes and approaches a steady state as the germanium concentration rises. The surface's decreased resistance, which makes it simpler to remove the convexity and concavity layers, is what causes the first rise in rate of wear. Until the rate of wear stabilizes, signifying the achievement of a

Table 4. The mechanical properties result at (10N & 20N).

Al_2O_3 (%)	HB (Kg/mm^2)	Rate of Wear (cm^3/N.M) at 30min		Enhancement rate (%) at
		10N	20N	20N
0	186	$2.20\text{ x}10^6$	$4.10\text{ x}10^6$	
0.5% Al_2O_3	195	$1.67\text{ x}10^6$	$2.40\text{ x}10^6$	48.52
1% Al_2O_3	213	$1.25\text{ x}10^6$	$1.15\text{ x}10^6$	75.56
1.5% Al_2O_3	227	$3.47\text{ x}10^7$	$6.53\text{ x}10^7$	84.28
2% Al_2O_3	238	$2.33\text{ x}10^7$	$4.74\text{ x}10^7$	87.73
2.5% Al_2O_3	249	$1.22\text{ x}10^7$	$2.70\text{ x}10^7$	88.62
3% Al_2O_3	258	$5.98\text{ x}10^8$	$8.94\text{ x}10^8$	92.85
3.5% Al_2O_3	262	$1.40\text{ x}10^8$	$8.44\text{ x}10^8$	92.9
4% Al_2O_3	273	$5.90\text{ x}10^9$	$1.6\text{ x}10^8$	93.71
4.5% Al_2O_3	288	$5.75\text{ x}10^9$	$1.36\text{ x}10^8$	97.94
5% Al_2O_3	295	$5.34\text{ x}10^9$	$1.26\text{ x}10^8$	98.84

constant coefficient of friction, this procedure is repeated.

Under constant load time and (20N and 30min), the Ti12Mo alloy and Ti12Mo alloy with Al_2O_3 addition rate of wear decreases with increasing Ge amount. The 0.5% Alumina particles alloy rate of wear is ($2.23x10^{-6}$ cm^3/N.M) compared to that of Ti12Mo alloy ($4.10x10^{-6}$ cm^3/N.M), achieving an enhancement rate of (48.52%).The reinforcing impact of intermetallic compounds is responsible for the resistant to wear enhancement, which rises with increasing Alumina particle concentration until it reaches 98.84% at 5% Alumina particles. By minimizing porosity and increasing the alloy's hardness, the addition of alumina particles lowers the rate of wear. This is explained by the intermetallic compound's (Ti6 Al_2O_3) reinforcing action. Fig. 6 illustrates how the amount of alumina particles affects rate of wear.

CONCLUSION

The incorporation of alumina (Al_2O_3) particles significantly enhanced the corrosion resistance of the Ti–12Mo alloys, with the enhancement exhibiting a strong dependence on Al_2O_3 amount. A maximum corrosion resistance enhancement of 98.8% was achieved at 5 wt.% Al_2O_3, corresponding to an extremely low corrosion rate of 2.14×10^{-10} mpy, indicating the development of a highly stable and protective passive surface layer. The resistant to wear of the Ti–12Mo alloy was markedly improved by Al_2O_3 reinforcement, with a monotonic increase observed as the alumina amount increased. The highest enhancement in resistant to wear, reaching 98.84%, was recorded at 5 wt.% Al_2O_3, where the rate of wear was reduced to 1.26×10^{-8} cm^3/N·m, demonstrating the effectiveness of alumina particles in mitigating material removal under sliding conditions. The addition of Al_2O_3 particles to the Ti–12Mo matrix promoted the formation of the $Ti_6Al_2O_3$ intermetallic phase, which contributed to a substantial increase in hardness. As a result, the hardness of the composite reached approximately 295kg/mm^2 at 5 wt.% Al_2O_3, reflecting enhanced resistance to plastic deformation and improved load-bearing capability. The presence of Al_2O_3 particles also led to a pronounced reduction in residual porosity, decreasing to approximately 19.2% at 5 wt.% Al_2O_3. This densification effect played a critical role in suppressing electrolyte penetration and stabilizing the passive film, thereby contributing directly to the observed reduction in corrosion rate and overall enhancement in electrochemical performance.

CONFLICT OF INTEREST

The authors declare that there is no conflict of interests regarding the publication of this manuscript.

REFERENCES

1. Study of high temperature properties of mechanically alloyed aluminium-titanium alloys. Metal Powder Report. 1993;48(11):41.
2. Al Deen HHJJ, Hamza SJ. Experimental Study of the Electrochemical and Biological Properties of (Nb-1%Zr-xGe) Alloy for Biomedical Applications. Neuroquantology. 2022;20(2):288-301.
3. Nabaa S. Radhi NSRea, et al. Investigation Biomedical Corrosion of Implant Alloys in Physiological Environment. International Journal of Mechanical and Production Engineering Research and Development. 2018;8(4):247-256.
4. S. Radhi N, H. Jamal Al-Deen H, Safaa Hadi R, S. Al-Khafaji Z. Investigate The Applicability of Coating Titanium Substrate by Hydroxyapatite for Surgical Implants. International Journal of Integrated Engineering. 2024;16(5).
5. Eman Yasir H, Jassim MSA-M, Nabaa Sattar R, Zainab A-K. Surface Modification of Titanium Alloy by Titania/Silver Multilayers Coating for Biomedical Application. Journal of Advanced Research in Micro and Nano Engieering. 2024;20(1):66-78.
6. Radhi NS, Salman AJ, Al-Khafaji Z. Investigation of in vitro behavior of composite coating hydroxyapatite-nano silver on 316L stainless steel substrate by electrophoretic technic for biomedical tools. Open Engineering. 2024;14(1).
7. Aubad MJ, Khafaji SOW, Hussein MT, Al-Shujairi MA. Modal analysis and transient response of axially functionally graded (AFG) beam using finite element method. Materials Research Express. 2019;6(10):1065g1064.
8. Bahl S, Suwas S, Chatterjee K. Comprehensive review on alloy design, processing, and performance of β Titanium alloys as biomedical materials. Int Mater Rev. 2020;66(2):114-139.
9. Khosravi R. Additively Manufactured Dental Appliances. Additive Manufacturing in Biomedical Applications: ASM International; 2022. p. 466-471.
10. Calazans Neto JV, Celles CAS, de Andrade CSAF, Afonso CRM, Nagay BE, Barão VAR. Recent Advances and Prospects in β-type Titanium Alloys for Dental Implants Applications. ACS Biomaterials Science and Engineering. 2024;10(10):6029-6060.
11. Pani D, Chattree A, Gupta J, Nene SS, Singh J. Mechanical and Corrosion Properties of Novel β-Ti-Rich Compositionally Complex Alloys in the As-Cast State. J Mater Eng Perform. 2025;35(10):10202-10217.
12. Sun C, Xiao R, Li H, Ruan Y. Effects of phase selection and microsegregation on corrosion behaviors of Ti-Al-Mo alloys. Corros Sci. 2022;200:110232.
13. El-Bagoury N, Ahmed SI, Ahmed Abu Ali O, El-Hadad S, Fallatah AM, Mersal GAM, et al. The Influence of Microstructure on the Passive Layer Chemistry and Corrosion Resistance for Some Titanium-Based Alloys.

Materials. 2019;12(8):1233.
14. Davoodi E, Montazerian H, Mirhakimi AS, Zhianmanesh M, Ibhadode O, Shahabad SI, et al. Additively manufactured metallic biomaterials. Bioactive Materials. 2022;15:214-249.
15. Esposito CI, Walter WL, Roques A, Tuke MA, Zicat BA, Walsh WR, et al. Wear in alumina-on-alumina ceramic total hip replacements. The Journal of Bone and Joint Surgery British volume. 2012;94-B(7):901-907.
16. Abakay E, Armağan M, Yıldıran Avcu Y, Guney M, Yousif BF, Avcu E. Advances in improving tribological performance of titanium alloys and titanium matrix composites for biomedical applications: a critical review. Frontiers in Materials. 2024;11.
17. The fibre/matrix interfacial shear strength in titanium alloy matrix composites reinforced by silicon carbide or boron CVD filaments. Composites. 1990;21(1):92.
18. Zhang M, Ma D, Wang J, Dai S, Xue Y, Zhu L. Enhancing interfacial bonding in metal matrix composites: challenges, methods, and future prospects. Crit Rev Solid State Mater Sci. 2025:1-54.
19. Sousa L, Basilio L, Alves AC, Toptan F. Tribocorrosion-resistant biofunctionalized Ti-Al2O3 composites. Surf Coat Technol. 2021;420:127329.
20. Barbis DP, Gasior RM, Walker GP, Capone JA, Schaeffer TS. Titanium powders from the hydride–dehydride process. Titanium Powder Metallurgy: Elsevier; 2015. p. 101-116.
21. Radhi NS, Nattah AM, Al-Khafaji ZS. Identify the effect of Fe_2O_3 nanoparticles on mechanical and microstructural characteristics of aluminum matrix composite produced by powder metallurgy technique. Open Engineering. 2024;14(1).
22. Fang ZZ, Paramore JD, Sun P, Chandran KSR, Zhang Y, Xia Y, et al. Powder metallurgy of titanium – past, present, and future. Int Mater Rev. 2017;63(7):407-459.
23. Zhang LC, Chen LY. A Review on Biomedical Titanium Alloys: Recent Progress and Prospect. Adv Eng Mater. 2019;21(4).
24. Zhou YL, Niinomi M, Akahori T, Fukui H, Toda H. Corrosion resistance and biocompatibility of Ti–Ta alloys for biomedical applications. Materials Science and Engineering: A. 2005;398(1-2):28-36.
25. Wang Z, Tan Y, Li N. Powder metallurgy of titanium alloys: A brief review. J Alloys Compd. 2023;965:171030.
26. Sousa L, Antunes RDM, Fernandes JCS, Alves AC, Toptan F. Influence of Al_2O_3 reinforcements and Ti-Al intermetallics on corrosion and tribocorrosion behavior of titanium. Surf Coat Technol. 2023;470:129835.
27. Practice for Microetching Metals and Alloys. ASTM International. http://dx.doi.org/10.1520/e0407-99
28. Gordin DM, Gloriant T, Nemtoi G, Chelariu R, Aelenei N, Guillou A, et al. WITHDRAWN: Synthesis, structure and electrochemical behavior of a beta Ti–12Mo–5Ta alloy as new biomaterial. Mater Lett. 2005;59(23):2959-2964.
29. Duerig T, Pelton A, Stöckel D. An overview of nitinol medical applications. Materials Science and Engineering: A. 1999;273-275:149-160.
30. Houdková Š, Kašparová M, Zahálka F. The friction properties of the HVOF sprayed coatings suitable for combustion engines, measured in compliance with ASTM G-99. WIT Transactions on Engineering Sciences; 2010/04/22: WIT Press; 2010. p. 129-139.
31. Şimşek I, Özyürek D. Investigation of Wear and Corrosion Behaviors of Ti15Mo Alloy Produced by Mechanical Alloying Method in SBF Environment. Powder Metall Met Ceram. 2019;58(7-8):446-454.
32. Moorhead PE. Tensile and Creep Properties of Columbium, Tantalum, and Titanium Alloys at Elevated Temperatures. Defense Technical Information Center; 1962 1962/12/10.